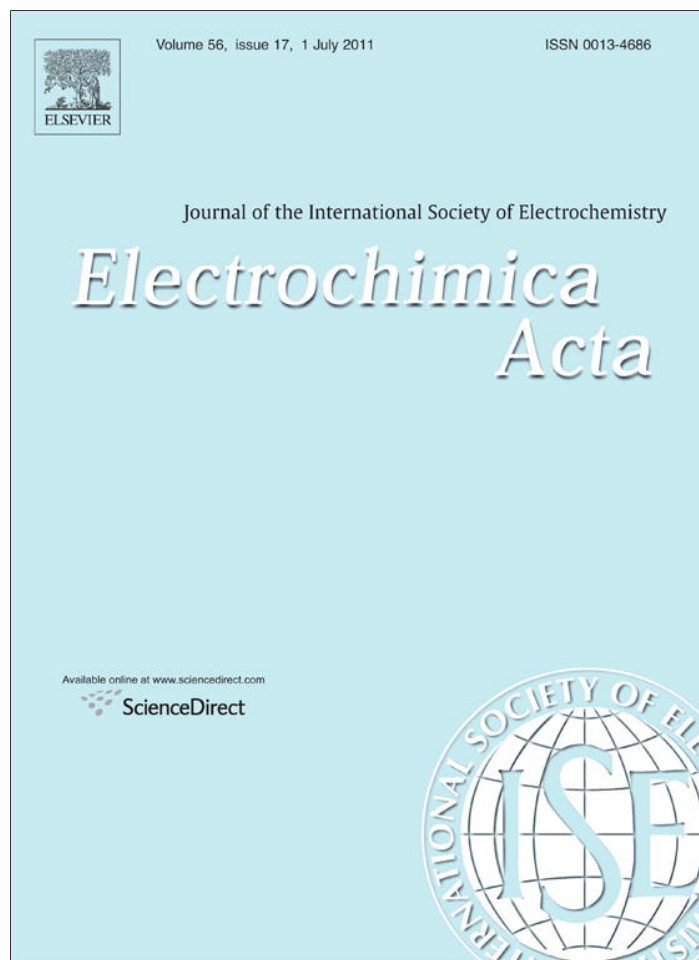


Provided for non-commercial research and education use.
Not for reproduction, distribution or commercial use.



This article appeared in a journal published by Elsevier. The attached copy is furnished to the author for internal non-commercial research and education use, including for instruction at the authors institution and sharing with colleagues.

Other uses, including reproduction and distribution, or selling or licensing copies, or posting to personal, institutional or third party websites are prohibited.

In most cases authors are permitted to post their version of the article (e.g. in Word or Tex form) to their personal website or institutional repository. Authors requiring further information regarding Elsevier's archiving and manuscript policies are encouraged to visit:

<http://www.elsevier.com/copyright>



Simulation of electric double layer capacitors with mesoporous electrodes: Effects of morphology and electrolyte permittivity

Hainan Wang, Julian Varghese, Laurent Pilon*

University of California, Los Angeles, Henry Samueli School of Engineering and Applied Science, Mechanical and Aerospace Engineering Department, 420 Westwood Plaza, Los Angeles, CA 90095, USA

ARTICLE INFO

Article history:

Received 30 September 2010
Received in revised form 30 March 2011
Accepted 30 March 2011
Available online 30 April 2011

Keywords:

Electric double layer capacitors
Mesoporous electrode morphology
Specific area capacitance
Diffuse layer
Stern layer

ABSTRACT

This paper aims to numerically predict the capacitance of electric double layer capacitors (EDLCs) made of mesoporous electrodes consisting of closely packed monodispersed mesoporous carbon spheres in $(\text{C}_2\text{H}_5)_4\text{NBF}_4$ /propylene carbonate electrolyte. The model faithfully accounts for the electrode packing morphology and the dependency of electrolyte dielectric permittivity on local electric field. Three sphere packing morphologies were investigated, namely, simple cubic (SC), body-centered cubic (BCC), and face-centered cubic (FCC). A cylindrical mesopore in a mesoporous carbon sphere was also simulated. This study demonstrates that the field-dependent electrolyte dielectric permittivity significantly affects the predicted capacitance of EDLCs. Moreover, the Stern layer needs to be accounted for in order to match predicted specific area capacitance with experimental data. This study also establishes that, for all packing structures, larger sphere diameter results in larger electric field at the electrode surface and thus larger diffuse layer specific area capacitance. For sphere diameter less than 40 nm, SC packing had the largest electrolyte volume fraction. This provided more space for the electric potential to decrease resulting in larger electric field at the electrode surface and diffuse layer specific area capacitance compared with BCC and FCC packings. On the contrary, FCC features the smallest volume fraction resulting in the lowest surface electric field and diffuse layer specific area capacitance. The packing morphologies of electrode spheres were found to have no significant effect on the diffuse layer specific area capacitance for sphere diameter larger than 40 nm.

© 2011 Elsevier Ltd. All rights reserved.

1. Introduction

Electric double layer capacitors (EDLCs) have attracted significant attention due to their promises as energy storage systems for high power applications such as hybrid electric vehicles [1,2]. EDLCs store electric charges physically in the electric double layer formed at the electrode/electrolyte interfaces which are readily accessible to ions present in the electrolyte [1–3]. Fig. 1 shows a schematic of the electric double layer structure formed near the surface of the cathode. Solvated cations of diameter a migrate and adsorb to the electrode surface due to electrostatic forces. The Stern layer is defined as the compact layer of immobile ions strongly adsorbed to the electrode surface [4–7]. Beyond the Stern layer is the so-called diffuse layer where ions are mobile under the coupled influence of electrostatic forces and diffusion [4–7]. Because the charge is stored

physically in EDLCs, the charging/discharging process is rapid and highly reversible. Thus, the cycle life of EDLCs is essentially infinite [1,2]. However, the energy density of EDLCs is typically lower than that of batteries [1,2].

Electrodes in EDLCs are typically made of materials featuring both micropores and mesopores offering large surface area [1–3,8–11]. Research efforts have focused on increasing the energy density of EDLCs by increasing the surface area of porous electrodes and tailoring their morphology or pore size distribution [1–3,8–11]. For example, Liu et al. [12] synthesized highly ordered mesoporous carbon spheres arranged in a face-centered cubic structure and used them as electrodes for EDLCs. Mesopores with hexagonal cross-section existed in the carbon spheres and aligned toward the sphere center [12]. The diameters of the mesoporous carbon spheres and their mesopores were 250 nm and 10.4 nm, respectively while the total specific surface area was reported to be $601 \text{ m}^2/\text{g}$ [12]. The electrolyte was $(\text{C}_2\text{H}_5)_4\text{NBF}_4$ in propylene carbonate non-aqueous solution [12]. The capacitance of the mesoporous carbon spheres was measured using both cyclic voltammetry and galvanostatic charge/discharge. The capacitance measured by cyclic voltammetry at low scan rate (1 mV/s) was identical to results obtained using galvanostatic method [12]. The

* Corresponding author at: University of California, Los Angeles, Henry Samueli School of Engineering and Applied Science, Mechanical and Aerospace Engineering Department, 420 Westwood Plaza, Engineering IV, Room 37-132, Los Angeles, CA 90095-1597, USA. Tel.: +1 310 206 5598; fax: +1 310 206 2302.

E-mail address: pilon@seas.ucla.edu (L. Pilon).

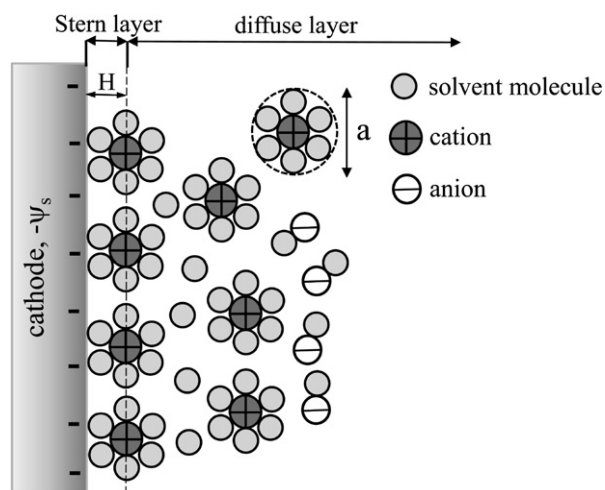


Fig. 1. A schematic of the electric double layer structure showing solvated anions and cations arrangement near the electrode/electrolyte interface in the Stern layer and the diffuse layer.

authors reported the specific area capacitance of 10.8, 12.6, and $14.0 \mu\text{F}/\text{cm}^2$ under voltage of 1.5V for the electrolyte concentrations of 0.3, 0.5, and 1.0 mol/L, respectively [12].

Numerous experimental studies have been devoted to characterizing the performances of EDLCs and their dependence on the material, morphology, and pore size of the porous electrodes, as well as on the ion size and solvent of the electrolyte [13–26]. It is believed that the optimal electrode morphology should provide both large surface area and “appropriate pore size” [1,9]. However, it remains unclear how the electrode morphology affects the capacitance of EDLCs [1,27,28].

The equivalent RC circuit models [29–32] and homogeneous models [33–46] have been used to numerically predict and investigate the performance of EDLCs. However, the equivalent RC circuit models require prior knowledge of macroscopic parameters such as the resistance and capacitance of the device which are typically determined experimentally or by other methods. Moreover, the classical RC circuit models may not be valid for EDLCs since this approach inherently neglects ion diffusion and non-uniform ion concentration in the electrolyte [47–49]. Alternatively, homogeneous models were also developed to investigate the charging/discharging dynamics of EDLCs. These models treat the heterogeneous microstructure of the electrodes as homogeneous with some effective macroscopic properties determined from effective medium approximations and depending on porosity and specific area [33–46]. In addition, they typically impose specific area capacitance or volumetric capacitance rather than predict them [33–46]. In addition, none of the RC and homogeneous models mentioned accounts for the detailed mesoporous electrode morphology.

Moreover, Yang et al. [50] performed molecular dynamics (MD) simulations of EDLCs made of 390 single-wall carbon nanotubes with diameter of 0.67 nm. Their results showed that the capacitance increases “modestly” with decreasing pore diameter larger than 2 nm. This qualitatively supported the experimental results reported for mesoporous carbide-derived carbon electrodes [18]. However, MD simulations are inadequate to perform extensive and systematic study of EDLCs due to their computational cost and time requirement.

This paper aims to clarify the fundamental physical mechanisms to be accounted for in simulating EDLCs. Three-dimensional (3D) equilibrium and heterogeneous model based on continuum theory was developed to predict the specific area capacitance of electrodes made of closely packed spheres and of cylindrical mesopores

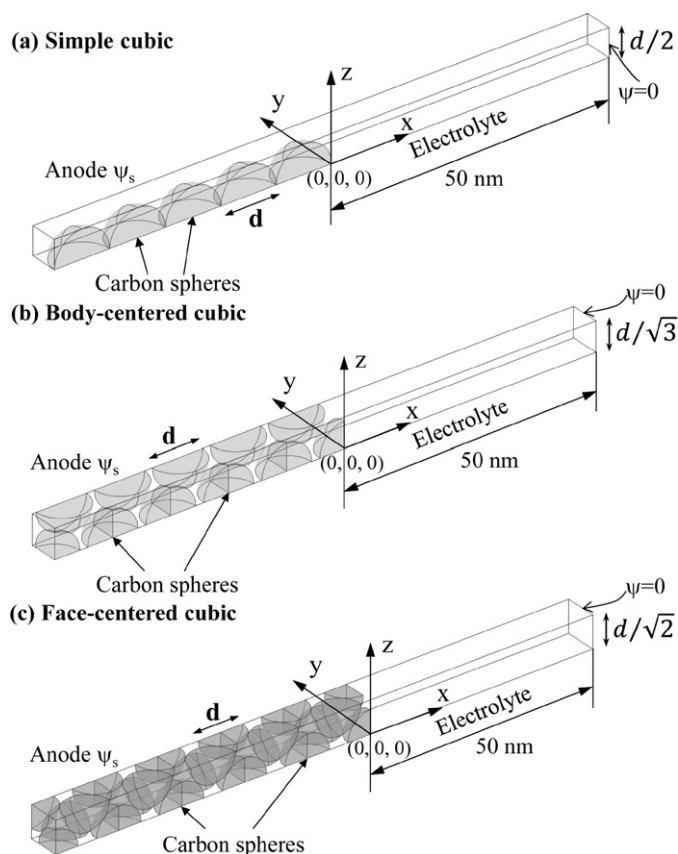


Fig. 2. Schematic, dimensions, and coordinate system of the computational domain simulated for carbon spheres with (a) SC, (b) BCC, and (c) FCC packings. Shaded areas represent carbon spheres of diameter d . Five unit cells are shown here for illustration purposes.

immersed in an electrolyte. It is unique in that it accounts for (i) the accurate electrode morphology, (ii) the non-uniform ion concentration and electric potential distribution in the electrolyte, as well as (iii) the dependency of the electrolyte dielectric permittivity on the electric field.

2. Analysis

2.1. Schematics and assumptions

The actual geometry of the mesoporous carbon electrodes synthesized in Ref. [12] was quite complex. In order to simplify the simulations while accurately accounting for the electrode morphology, the problem was divided in two uncoupled problems simulating (1) non-porous (i.e. dense) carbon spheres arranged in periodic packing, and (2) a single mesopore inside a carbon matrix. This approach is supported by the following facts: (i) under equilibrium conditions, the electric potential is uniform across all the electrode particles. Thus, the electric potentials at the outer surface of the carbon spheres and the inner pore walls were identical. (ii) The electric potential in the electrolyte solution decreased rapidly to zero away from the electrode surface as discussed in Section 3.2. Therefore, it suffices to consider the dense spheres and mesopores separately while imposing the same potential at the sphere or mesopore surface and zero potential far-away in the electrolyte solution.

Fig. 2 shows the schematic of a representative computational domain of closely packed dense spheres. Only the domain consisting of the electrodes and the electrolyte solution was considered thus, ignoring the current collector. The electrodes consisted of

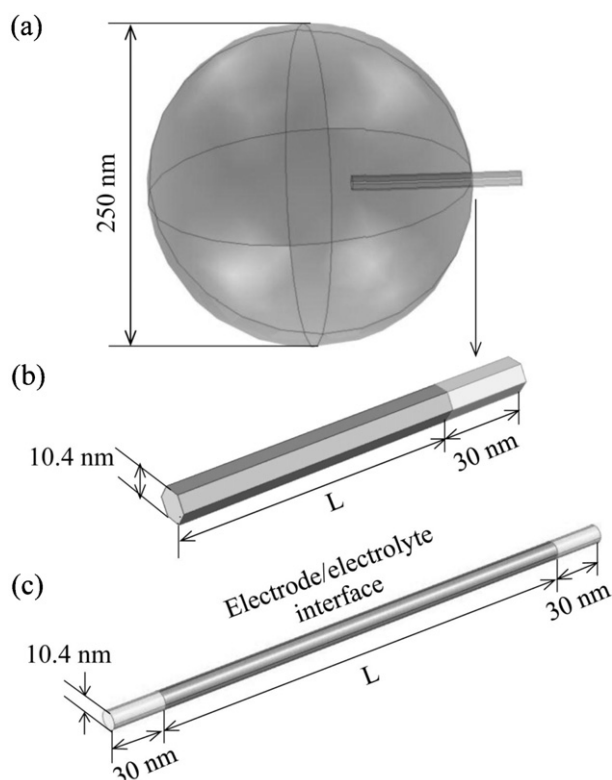


Fig. 3. Schematic and dimensions of the computational domain simulated for (a) one mesopore within a carbon sphere of (b) hexagonal cross-section with pore length $L < 250$ nm, and (c) circular cross-section with pore length $L = 250$ nm.

dense monodispersed carbon spheres arranged in simple cubic (SC), body-centered cubic (BCC), and face-centered cubic (FCC) packings. Due to the periodicity, only a representative region of the entire electrode was considered with the width and height equal to that of one unit cell. Moreover, only a quadrant of a lattice unit cell was simulated by virtue of symmetry (Fig. 2). Fig. 2a–c illustrates the computational domain corresponding to five unit cells with SC, BCC and FCC packings, respectively. The distance separating the anode and cathode (separator) was always specified as 100 nm. Increasing the distance to 200 nm was found to have no effect on the predicted equilibrium capacitance. Note, however, that this distance would have a significant effect on transient simulations of the EDLC devices [40,41,51]. In addition, it is sufficient to simulate only half of the entire device and consider only the anode, for example, due to antisymmetry in the electric potential.

Moreover, Fig. 3 shows the schematic of the computational domain of one mesopore in a mesoporous carbon sphere. Assuming the electric potential to be the same across the solid phase of the mesoporous spheres, it suffices to simulate only one mesopore. Mesopores with either hexagonal or circular cross-section were simulated. The length of the mesopore was denoted by L and varied from 50 to 250 nm since its exact length remained unknown [12]. An additional electrolyte region was specified on one end of the mesopore with $L < 250$ nm corresponding to the space between adjacent carbon spheres (Fig. 3b). Due to symmetry, the length of this region was specified as 30 nm corresponding to half of the “interconnected window” between carbon spheres of 250 nm in diameter [12]. For mesopores going through the entire sphere ($L = 250$ nm), a 30 nm thick electrolyte region was specified at both ends of the pore (Fig. 3c).

To make the problem mathematically tractable, the following assumptions were made: (1) the electric potential and ion concentration were invariant with time (steady state) and reached their

equilibrium states, (2) all the electrode particles were at the same potential since there is no electric current under equilibrium conditions, (3) anions and cations had the same effective diameter [52–55], (4) isothermal conditions were assumed throughout the electrolyte solution and the carbon spheres, (5) advection of the electrolyte was assumed to be negligible, (6) the ions could only accumulate at the electrode surfaces and could not diffuse into the solid phase of carbon particles constituting the electrodes. In fact, in the cyclic voltammetry experiments reported in Ref. [12], no pseudocapacitive peak was observed in the C – V curves. Therefore, ion insertion contribution to the electrode capacitance was considered negligible [5,56], and (7) the continuum theory was assumed to be valid for all the cases considered in this study. Its validity has been examined in the literature [57–60] and is typically accepted when the pore diameter is larger than 3–5 nm [57–60].

2.2. Governing equation and boundary conditions

Based on assumptions (2) and (6), the governing equations only need to be solved within the electrolyte solution. The local steady-state and equilibrium electric potential in the diffuse layer, denoted by $\psi(x, y, z)$, can be found by solving the modified Poisson–Boltzmann (MPB) model accounting for the finite size of the ions [52–55,61]. Among different MPB models, Bikerman’s model was the simplest developed for binary and symmetric electrolytes and was expressed as [52–55,61],

$$\nabla \cdot (\epsilon_0 \epsilon_r \nabla \psi) = zeN_A c_\infty \frac{2 \sinh(ze\psi/k_B T)}{1 + 2\nu \sinh^2(ze\psi/2k_B T)} \quad (1)$$

where ϵ_0 and ϵ_r are the free space permittivity and relative permittivity of the electrolyte, respectively. The valency of the symmetric electrolyte is denoted by z , while T is the absolute temperature, c_∞ is the bulk molar concentration of electrolyte, e is the elementary charge, N_A and k_B are the Avogadro constant and Boltzmann constant, respectively. The packing parameter is defined as $\nu = 2a^3 N_A c_\infty$ where a is the effective ion diameter. It represents the ratio of the total bulk ion concentration to the maximum ion concentration assuming a simple cubic ion packing [49,54,55,62]. Therefore, it should not be larger than unity for the model to be physically acceptable [49,62].

The boundary conditions associated with Eq. (1) correspond to experimental conditions where the electric potential was set to be constant and equal to ψ_s and $-\psi_s$ at the anode and cathode, respectively. By virtue of symmetry of the geometry and antisymmetry in the electric potential, only half of the entire domain was simulated (Fig. 2). Then, the boundary conditions can be written as,

$$\psi(\mathbf{r}_a) = \psi_s \quad \text{and} \quad \psi(\mathbf{r}_s) = 0 \quad (2)$$

where \mathbf{r}_a and \mathbf{r}_s denote the position vectors of the electrode/electrolyte interfaces for the anode and the center plane of the separator, respectively. In addition, symmetric conditions were imposed at all the other boundaries.

2.3. Constitutive relations

In order to solve Eqs. (1) and (2), the electrolyte properties ϵ_r , z , c_∞ and a are needed. The relative permittivity ϵ_r of polar electrolytes may significantly decrease as the electric field increases [63–67]. In fact, the individual electrolyte molecules become highly oriented under large electric field. Therefore, further orientation of the molecules can hardly provide more polarization and the relative permittivity decreases [63–65]. Here, the Booth model [65–67] was used to account for the effects of the electric field on electrolyte

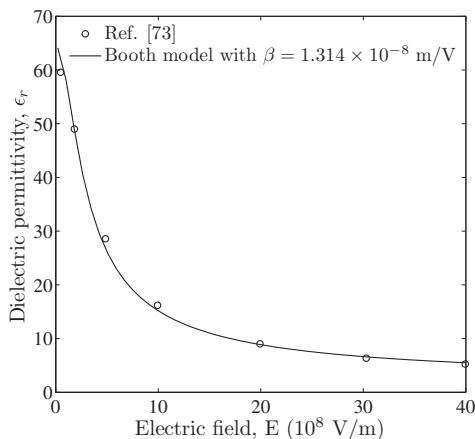


Fig. 4. Comparison of the relative permittivity of propylene carbonate electrolyte predicted by Booth model [Eq. (3)] with $\beta = 1.314 \times 10^{-8}$ m/V with predictions from MD simulations reported in Ref. [73]. The maximum relative difference was less than 7%.

relative permittivity. It is expressed as [65–67],

$$\epsilon_r(E) = n^2 + (\epsilon_r(0) - n^2) \frac{3}{\beta E} \left[\coth(\beta E) - \frac{1}{\beta E} \right] \quad \text{for } E \geq 10^7 \text{ V/m} \quad (3a)$$

$$\epsilon_r = \epsilon_r(0) \quad \text{for } E < 10^7 \text{ V/m} \quad (3b)$$

where $E = |-\nabla\psi|$ is the norm of the local electric field vector, $\epsilon_r(0)$ is the relative permittivity at zero electric field, and n is the index of refraction of the electrolyte at zero electric field frequency.

The Booth model was combined with Poisson equation in Refs. [68–70] to investigate the repulsion between two charged planar surface electrodes due to hydration forces in aqueous electrolyte solutions. However, to the best of our knowledge, the present study is the first to combine field-dependent permittivity and Poisson equation for simulating EDLCs. It focuses on $(\text{C}_2\text{H}_5)_4\text{NBF}_4$ electrolyte in propylene carbonate solution at room temperature characterized by the following properties: $\epsilon_r(0) = 64.4$ [71], $n = 1.42$ [72], and $z = 1$. Moreover, the parameter β in Eq. (3a) was determined by least-square fitting for the relative permittivity of propylene carbonate reported in Ref. [73] and obtained by MD simulations. Fig. 4 shows the relative permittivity of propylene carbonate predicted by the Booth model with $\beta = 1.314 \times 10^{-8}$ m/V along with the predictions from MD simulations [73]. The maximum relative difference was found to be less than 7% for electric field between 0 and 4×10^9 V/m.

Finally, the values of electrolyte concentration c_∞ used in the simulation were the same as those used in Ref. [12], i.e., $c_\infty = 1.0$ mol/L. The ion diameter of non-solvated $(\text{C}_2\text{H}_5)_4\text{N}^+$ and BF_4^- ions was reported to be $a_{\min} = 0.68$ nm and 0.33 nm [74,18], respectively. However, as discussed in Refs. [55,75], “Smaller bare ions tend to be more heavily solvated and therefore have larger effective diameters”. Here, the effective ion diameters of $(\text{C}_2\text{H}_5)_4\text{N}^+$ and BF_4^- were assumed to be equal. In addition, when the electrolyte concentration decreases, the dissolved electrolyte ions are more solvated, i.e., they are surrounded by more solvent molecules [12,76–79]. Consequently, the effective diameter a of the ions may decrease with increasing electrolyte concentration [12,77,79]. Considering the fact that the solubility of $(\text{C}_2\text{H}_5)_4\text{NBF}_4$ in propylene carbonate is about 1 mol/L at room temperature [80], the effective ion diameter a was assumed to be equal to $a = 0.68$ nm. The other parameters needed to perform the simulations were also chosen

to be consistent with those used experimentally, i.e., $T = 298$ K, and $2\psi_s = 1.5$ V [12].

2.4. Method of solution and data processing

Eq. (1) was solved using the commercial finite element solver COMSOL 3.5a, along with the boundary conditions given by Eq. (2). The model was solved for constant permittivity $\epsilon_r(0)$ or field-dependent permittivity $\epsilon_r(E)$ given by Eq. (3). The simulations were run on a Dell workstation Precision 690 with two 2.66 GHz Quad-Core Intel Xeon CPUs and 40 GB of RAMs.

The total charge Q stored at the anode was computed by integrating the surface charge density ($\epsilon_0\epsilon_r\mathbf{E} \cdot \mathbf{n}$) along the anode/electrolyte interfaces as [6,81],

$$Q = \int_{A_a} \epsilon_0\epsilon_r\mathbf{E} \cdot \mathbf{n} dA \quad (4)$$

where $\mathbf{E} = -\nabla\psi$ is the electric field vector, \mathbf{n} is the local outward normal unit vector at the anode/electrolyte interfaces. The interfacial surface area A_a of dense sphere packings was the sum of the surface area of the carbon spheres and of the current collector. For the single pore simulations, A_a was the surface area of the mesopore. The absolute charge computed at the anode and cathode was identical due to symmetry in geometry and to the anti-symmetry of the electric potential. The capacitance of the diffuse layer of the simulated EDLC from single electrode was estimated as $C^D = Q/\psi_s$ while its specific area capacitance C_s^D was given by,

$$C_s^D = \frac{C^D}{A_a} = \frac{Q}{\psi_s A_a} = \frac{1}{\psi_s A_a} \int_{A_a} \epsilon_0\epsilon_r\mathbf{E} \cdot \mathbf{n} dA \quad (5)$$

Moreover, the total specific area capacitance of electric double layer, denoted by C_s , consists of the Stern layer capacitance and of the diffuse layer capacitance in series. It is expressed as [5,7,56],

$$\frac{1}{C_s} = \frac{1}{C_s^{\text{St}}} + \frac{1}{C_s^D} \quad (6)$$

where C_s^{St} is the Stern layer specific area capacitance which can be estimated as [5,7,56],

$$C_s^{\text{St}} = \frac{\epsilon_0\bar{\epsilon}_r}{H} \quad (7)$$

where H is the thickness of the Stern layer. It can be approximated as the radius of the solvated ions [4–7] while $\bar{\epsilon}_r$ is the average dielectric permittivity along electrode surface defined as,

$$\bar{\epsilon}_r = \frac{1}{A_a} \int_{A_a} \epsilon_r(E) dA \quad (8)$$

Here, $\epsilon_r(E)$ is determined by Eq. (3) based on the local electric field at the electrode surface computed numerically. Note that, the potential drop in the Stern layer was neglected. The same approach was used by Bazant et al. [55] to predict the differential double layer capacitance of Ag electrode in KPF_6 aqueous electrolyte solution.

Finally, numerical convergence was assessed based on the total charge Q accumulated at the electrode/electrolyte interfaces. For the simulation of packed carbon spheres, the convergence criterion was chosen such that the maximum relative difference in Q was less than 2% and 6% for constant permittivity and field-dependent permittivity, respectively, when multiplying the total number of finite elements by at least two. For the simulation of mesopores, this convergence criterion was chosen to be 2.5% for both constant and field-dependent dielectric permittivity. The tetrahedral elements were used in all the meshes generated. Mesh refinement was required near the electrode surfaces where the potential gradient was large. The maximum element size to reach a converged solution was about 0.08–0.2 nm at all electrode surfaces.

The total number of finite elements depended on the electrode morphology (SC, BCC, FCC) and on the number of unit cells simulated, as well as on the model used for ϵ_r . The number of finite elements was on the order of 10^5 to 10^6 in the simulations of densely packed spheres when assuming constant ϵ_r . It was one order of magnitude larger for field-dependent ϵ_r predicted by Eq. (3) due to larger potential gradient near the electrode surface as discussed in Section 3.3. In addition, the number of elements was on the order of 10^5 to 10^6 for the single-pore simulations depending on the pore length and for both constant and field-dependent ϵ_r .

3. Results and discussions

3.1. Effect of electrode thickness on diffuse layer capacitance

The effect of the number of unit cells on the diffuse layer specific area capacitance C_s^D was first investigated for SC, BCC, and FCC packings and for electrode spheres with diameter equal to 5, 10, 20, 40, 60, 80 and 100 nm. For each packing morphology and sphere diameter, the number of unit cells was increased from 1 to 5. The diffuse layer specific area capacitance C_s^D computed when assuming constant electrolyte permittivity decreased slightly when increasing the number of unit cells and rapidly reached a plateau (not shown). The effect of the number of unit cells simulated on C_s^D was smaller for large particle diameter. In fact, for particle diameter $d=20$ nm, the relative difference in C_s^D between 2 and 5 unit cells was found to be less than 2%.

In cases when ϵ_r dependency on electric field was accounted for through Eq. (3), this difference was less than 3% for all sphere diameters and packing morphologies considered. Therefore, the diffuse layer specific area capacitance C_s^D computed for mesoporous electrodes can be assumed to be independent of the number of unit cells simulated.

3.2. Effect of electrode morphology

Fig. 5 shows the computed electric potential contours in two representative cross-sections perpendicular to the x -axis in the computational domain for the SC packing with five spheres of diameter $d=10$ nm. Their x -coordinates were (a) $x=-d/2$, and (b) $x=-d$, respectively. Results were obtained assuming constant permittivity ($\epsilon_r=64.4$), $c_\infty=1$ mol/L, $a=0.68$ nm and $\psi_s=0.75$ V. Fig. 5 demonstrates that the electric potential decreased rapidly to zero away from the electrode surface. Note that the nearly identical contours were observed periodically along the x -axis for $-5d < x < 0$ (Fig. 2a).

Fig. 6 shows the computed diffuse layer specific area capacitance C_s^D for sphere diameter ranging from 5 to 100 nm obtained assuming constant permittivity ($\epsilon_r=64.4$), $c_\infty=1$ mol/L, and $a=0.68$ nm for SC, BCC, and FCC packings. It is evident that C_s^D increased with particle diameter for all three morphologies simulated and rapidly reached a plateau. This can be attributed to the fact that (i) the electric potential ψ in the electrolyte solution was maximum at the electrode surface and decreased rapidly away from it, (ii) the electric double layer of adjacent spheres started overlapping as the particles got closer to one another, and (iii) the distance between surfaces of adjacent electrode particles increased with particle diameter. Overall, larger electrode particle diameter resulted in larger electric field ($\mathbf{E}=-\nabla\psi$) at the electrode surface and thus larger C_s^D , according to Eq. (5). The asymptotic value of C_s^D , represented by the solid line in Fig. 6, corresponds to that of planar

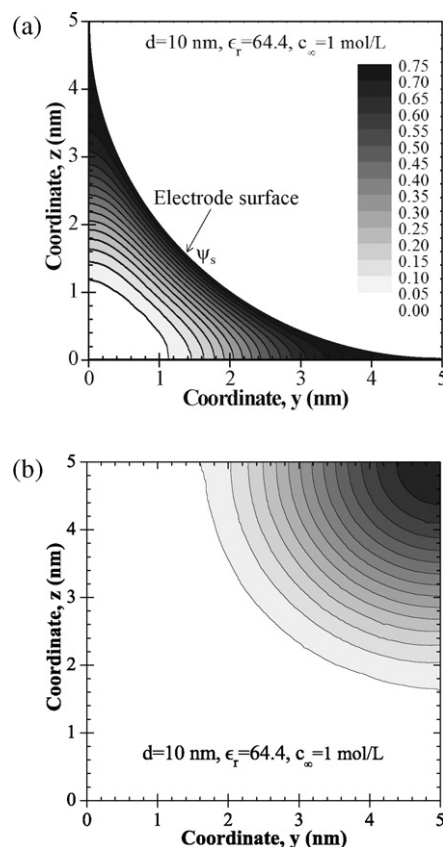


Fig. 5. Numerically predicted electric potential contours at two representative cross-sections perpendicular to the x -axis for the SC packing with five spheres with diameter of $d=10$ nm. Their x -coordinates were (a) $x=-d/2$, and (b) $x=-d$. Electrolyte concentration was set as $c_\infty=1.0$ mol/L, electrolyte permittivity was assumed to be constant ($\epsilon_r=64.4$), $a=0.68$ nm and $\psi_s=0.75$ V.

electrodes assuming constant electrolyte permittivity and given by [54,55,62],

$$C_s^D = \frac{2zeN_A c_\infty \lambda_D}{\psi_s} \sqrt{\frac{2}{v} \log \left[1 + 2v \sinh^2 \left(\frac{ze\psi_s}{2k_B T} \right) \right]} \quad (9)$$

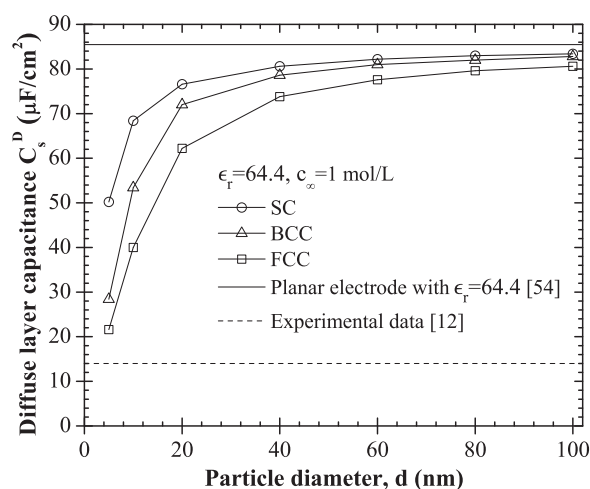


Fig. 6. Numerically predicted diffuse layer specific area capacitance C_s^D for SC, BCC, and FCC packings. Electrolyte concentration was set as $c_\infty=1.0$ mol/L, electrolyte permittivity was assumed to be constant ($\epsilon_r=64.4$) and $a=0.68$ nm. Solid line represents the theoretical value of C_s^D for planar electrodes given by Eq. (9) [54]. Dashed line shows experimental data reported for identical electrolyte and mesoporous carbon spheres with 250 nm in diameter in a FCC packing [12].

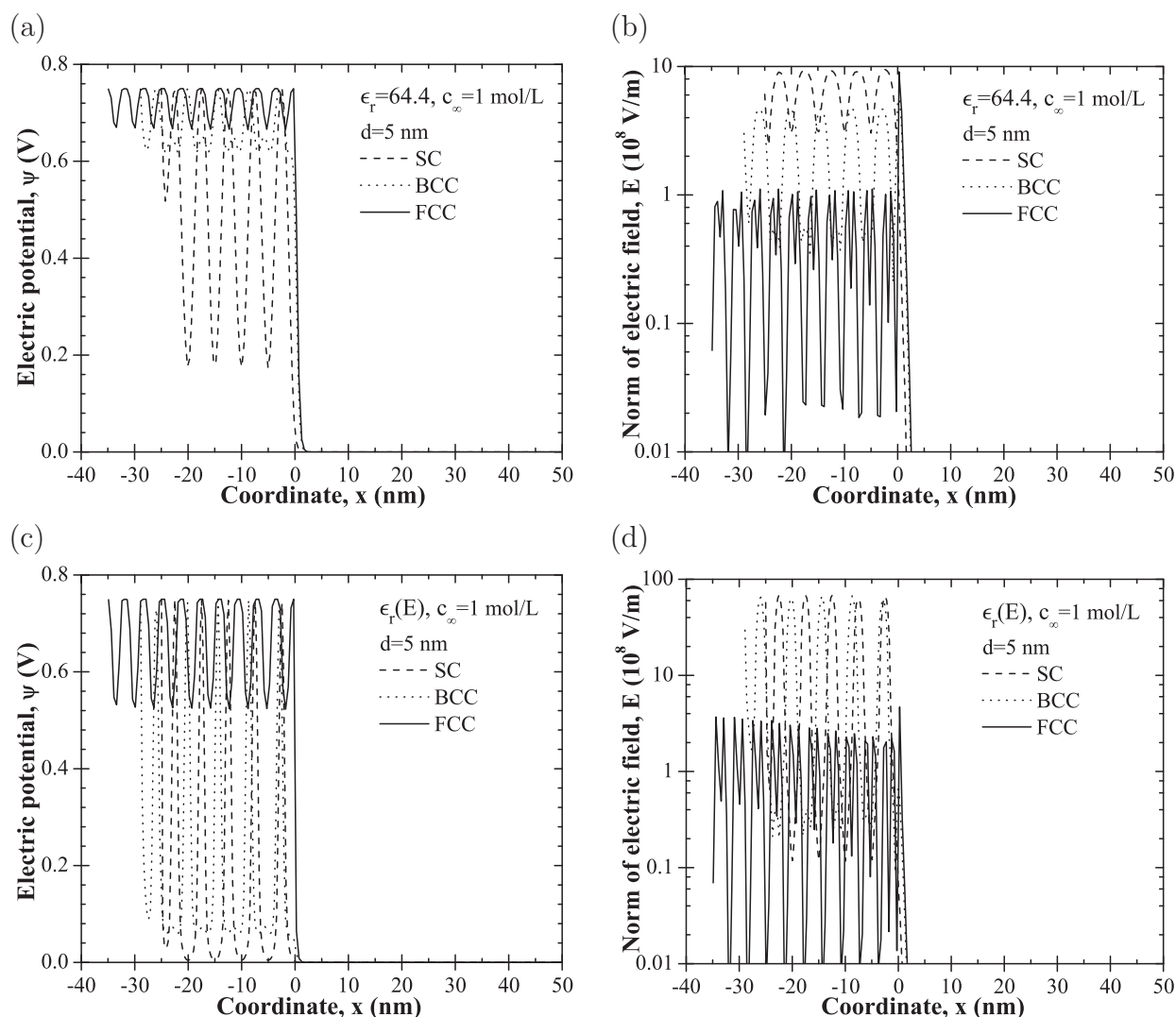


Fig. 7. Numerically predicted electric potential ψ and norm of electric field ($E = |-\nabla\psi|$) as a function of x along a straight line for SC, BCC, and FCC packings with five unit cells and spheres of 5 nm in diameter. Results were obtained using (a, b) constant permittivity ($\epsilon_r = 64.4$), and (c, d) field-dependent permittivity given by Eq. (3) with electrolyte concentration $c_\infty = 1.0$ mol/L, and $a = 0.68$ nm.

where λ_D is the Debye length for symmetric electrolyte defined as $\lambda_D = (\epsilon_0 \epsilon_r k_B T / 2e^2 z^2 N_A c_\infty)^{1/2}$ [6,54,55]. For the cases considered in Fig. 6, Eq. (9) predicts $C_s^D = 85.4 \mu\text{F}/\text{cm}^2$. In addition, the specific area A_s of the mesoporous electrode is defined as the total surface area A_d divided by the mass of the electrode and is expressed in m^2/g . It decreases with increasing particle diameter. Therefore, the numerical predictions in Fig. 6 were consistent with the experimental results reported in Ref. [17] showing that the total specific area capacitance C_s decreased with increasing specific area.

Moreover, for a given particle diameter, SC packing featured the largest diffuse layer specific area capacitance C_s^D and FCC packing the lowest (Fig. 6). Indeed, SC packing has the largest electrolyte volume fraction, thus it provides the largest inter-particle distance through which the electric potential decreases. This results in larger electric field and surface charge density at the electrode/electrolyte interfaces and consequently, larger diffuse layer specific area capacitance C_s^D compared with other packings. On the contrary, FCC packing has the lowest electrolyte volume fraction. Thus, it features the lowest electric field, surface charge density and diffuse layer specific area capacitance. To confirm this physical interpretation, Fig. 7a and b respectively shows the numerical predictions of the local electric potential and the norm of electric field vector along a straight line passing through SC, BCC and FCC

packings with five unit cells for sphere diameter $d = 5$ nm. For each packing morphology, the straight line was chosen such that it was parallel to the x -axis and touched the surface of the spheres. More specifically, the (y, z) coordinates of each plotting line were given by (i) $[(d/2)\cos 45^\circ, (d/2)\sin 45^\circ]$ for SC packing, (ii) $[d/2, 0]$ for BCC packing, and (iii) $[(d/2)\cos 45^\circ, (d/2)\sin 45^\circ]$ for FCC packing (see Fig. 1). The maximum value of the electric potential shown in Fig. 7a was 0.75 V corresponding to ψ_s at the surface of the electrode particles. Fig. 7a establishes that the electric potential varied significantly from 0.18 to 0.75 V between electrode spheres for SC packing while it oscillated only between 0.67 and 0.75 V for FCC packing. Consequently, the electric field was the largest between spheres with SC packing and the smallest between those with FCC packing as shown in Fig. 7b. Note also that the electric potential and electric field in the electrolyte decreased rapidly to zero away from the boundary of mesoporous electrodes located in the plane $x = 0$. Further increasing the separator thickness did not affect the electric potential profile at the electrode surface. Thus the predicted specific area capacitance C_s^D was independent of the separator thickness. Furthermore, Fig. 6 demonstrates that the difference in diffuse layer specific area capacitance C_s^D among the three morphologies decreased with increasing particle diameter. In fact, C_s^D reached nearly the same value for all morphologies

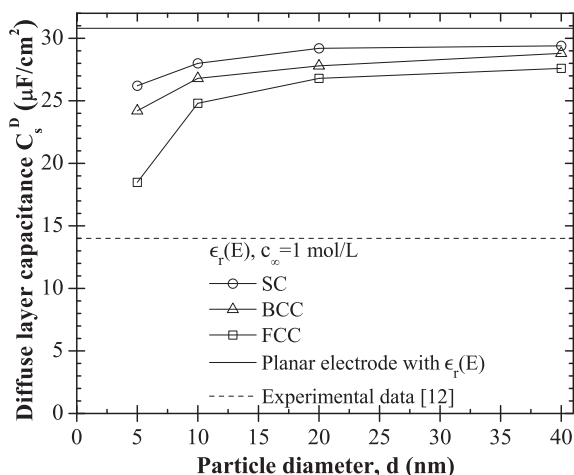


Fig. 8. Numerically predicted diffuse layer specific area capacitance C_s^D for SC, BCC, and FCC packings. Electrolyte concentration was set as $c_\infty = 1.0$ mol/L, electrolyte permittivity was given by Eq. (3) and $a = 0.68$ nm. Dashed line shows experimental data ($14.0 \mu\text{F}/\text{cm}^2$) reported for identical electrolyte and mesoporous carbon spheres with 250 nm in diameter in a FCC packing [12].

for particle diameter larger than 100 nm. This establishes that the packing of the electrode spheres has no significant effect on diffuse layer specific area capacitance for the electrode particle diameter larger than 100 nm when assuming constant electrolyte permittivity. However, note that the diffuse layer gravimetric capacitance $C_g^D (= C_s^D A_s)$ decreased with increasing particle diameter for all packing morphologies (not shown) due to the decrease in specific area. This is also consistent with experimental data for the total gravimetric capacitance reported in the literature [3,9,13,17,19,20,25].

3.3. Effect of electric field on dielectric permittivity

Fig. 7c and d respectively shows the electric potential and the norm of the electric field along the same lines as those previously discussed for SC, BCC, FCC structures. Here, the results were obtained using field-dependent dielectric permittivity given by Eq. (3) while all other parameters including $a = 0.68$ nm were identical to those used for results shown in Fig. 7a and b. The local electric potential and the norm of the electric field followed the same trend as that shown in Fig. 7a and b. However, the norm of electric field plotted in Fig. 7d was almost one order of magnitude larger than that obtained assuming constant electrolyte permittivity (Fig. 7b). This can be explained by examining Eq. (1). The term on the right-hand side was constant at the electrode/electrolyte interfaces where $\psi = \psi_s$. Therefore, the electric field ($\mathbf{E} = -\nabla\psi$) at the electrode/electrolyte interfaces, appearing on the left-hand side must increase to compensate for the decrease in dielectric permittivity ϵ_r at large electric field (Fig. 4).

Fig. 8 shows the computed diffuse layer specific area capacitance C_s^D obtained as a function of electrode particle diameter using field-dependent permittivity [Eq. (3)] as well as $c_\infty = 1$ mol/L and $a = 0.68$ nm for SC, BCC and FCC packings. The computed capacitance C_s^D followed the same trend as the results predicted assuming constant permittivity (Fig. 6) for all morphologies and particle diameters. However, it was significantly smaller when using field-dependent permittivity. In addition, C_s^D reached a plateau for smaller particle diameter around 40 nm instead of 100 nm when assuming constant permittivity. The asymptotic value of C_s^D , represented by the solid line in Fig. 8, corresponds to the diffuse layer specific area capacitance of a planar electrode. It was found to be $30.8 \mu\text{F}/\text{cm}^2$ using Eq. (5) after solving Eq. (1) combined with field-dependent permittivity [Eq. (3)]. For $d = 40$ nm, the maximum

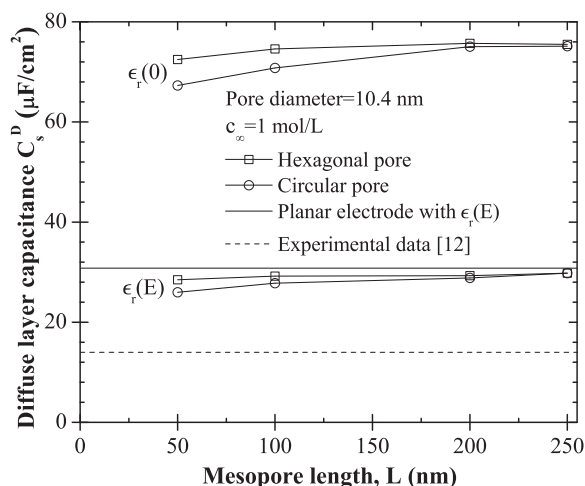


Fig. 9. Numerically predicted diffuse layer specific area capacitance C_s^D for one mesopore as a function of mesopore length assuming hexagonal and circular cross-section with diameter 10.4 nm. Electrolyte concentration was set as $c_\infty = 1.0$ mol/L, and $a = 0.68$ nm. Dashed line shows experimental data ($14.0 \mu\text{F}/\text{cm}^2$) reported for identical electrolyte and mesoporous carbon spheres with 250 nm in diameter in a FCC packing [12].

relative difference in C_s^D for the three morphologies was less than 6%. Here also, the effect of electrode packing morphology on the diffuse layer specific area capacitance can be neglected as the electrode particle diameter increases. Moreover, the value of C_s^D predicted for FCC packing of carbon spheres larger than 40 nm was found to be $27.6 \mu\text{F}/\text{cm}^2$.

Fig. 9 shows the computed diffuse layer specific area capacitance C_s^D of a mesopore with hexagonal or circular cross-section as a function of pore length obtained using constant and field-dependent electrolyte permittivity. It indicates that C_s^D slightly increased with pore length. Changing the pore cross-section from hexagonal to circular resulted in minor differences in C_s^D . This difference decreased with increasing pore length and was insignificant for pore longer than 100 nm. The diffuse layer specific area capacitance of hexagonal and circular pores predicted using field-dependent permittivity ranged from 26.0 to $29.8 \mu\text{F}/\text{cm}^2$. This was consistent with the diffuse layer specific area capacitance of $27.6 \mu\text{F}/\text{cm}^2$ predicted for carbon spheres arrays without mesopores arranged in FCC packing (Fig. 8). Here again, the numerical predictions assuming constant permittivity were significantly larger than the predictions using field-dependent permittivity. The solid line in Fig. 9 is the same asymptotic value of $C_s^D = 30.8 \mu\text{F}/\text{cm}^2$ for planar electrodes shown in Fig. 8. This demonstrates that the closely packed dense spheres and the mesopores feature the same diffuse layer specific area capacitance when the diameters of the electrode particles and of the mesopores are large enough regardless of the morphology and porosity.

3.4. Comparison with experimental data

The capacitance measured from cyclic voltammetry at small scan rate (e.g. <10 mV/s) is analogous to the equilibrium capacitance [12,51]. Therefore, the equilibrium capacitance computed using Eq. (6) can be directly compared with experimental results reported in Ref. [12] for the scan rate of 1 mV/s. In addition, previous discussion (Section 3.1) established that predicted total specific area capacitance of mesoporous electrodes with more than two unit cells can be compared with actual experimental data where electrodes were thick ($>20 \mu\text{m}$ [20–22]) and typically consisted of a large number of unit cells [12].

For FCC packing of dense spheres with diameter of 40 nm, Eq. (8) yields $\epsilon_r = 7.8$. Using $H = a/2 = 0.34$ nm as the Stern layer thickness, Eq. (7) predicted $C_s^{st} = 20.3 \mu\text{F}/\text{cm}^2$ while $C_s^D = 27.6 \mu\text{F}/\text{cm}^2$. Thus, the total specific area capacitance was $C_s = 11.8 \mu\text{F}/\text{cm}^2$. This value is similar to experimental measurements reporting $C_s = 14.0 \mu\text{F}/\text{cm}^2$ for mesoporous carbon spheres [12]. This demonstrates that the Stern layer capacitance needs to be accounted for in predicting the capacitance of EDLCs with large electrolyte concentrations and electric potentials such that $c_\infty \geq 1$ mol/L and $\psi_s \geq 0.5$ V.

Finally, one should be careful in extending the conclusions drawn from the present simulations to micropores with diameter less than 2 nm for the following two reasons: (i) the diffuse layer may not exist in such small pores and (ii) the continuum theory and the Bikerman model [Eq. (1)] may not be valid. In fact, Chmiola et al. [18] observed an anomalous increase in capacitance for the pore diameter less than 1 nm. This phenomenon was explained by the adsorption of desolvated ions in micropores [18,22]. In these conditions, atomistic simulations may be more appropriate such as that performed in Ref. [50].

4. Conclusion

This paper presented numerical simulations of EDLCs with electrodes made of closely packed monodispersed mesoporous spheres. For the first time, a 3D heterogeneous mesostructures were modeled based on continuum theory to investigate the capacitance of EDLCs while accounting for the accurate electrode morphology and the effect of electric field on electrolyte permittivity. To simplify the problem, both dense carbon spheres in SC, BCC, and FCC packings and a single mesopore with hexagonal and circular cross-sections in a carbon sphere were simulated. The following conclusions can be drawn:

1. The field-dependent permittivity $\epsilon_r(E)$ significantly affects the predicted diffuse and Stern layer capacitances of EDLCs.
2. The Stern layer capacitance needs to be accounted for in order to find good agreement between the predicted and the experimental specific area capacitance [12] for high electrolyte concentrations and electric potentials typically encountered in EDLCs.
3. For a given sphere packing, the diffuse layer specific area capacitance increased with increasing diameter. Larger spheres provided more space for the electric potential to decrease resulting in larger electric field at the electrode surface, and therefore larger diffuse layer specific area capacitance.
4. The electrode morphology (SC, BCC, FCC) was found to have no significant effect on the diffuse layer specific area capacitance for sphere diameter larger than 40 nm.
5. SC packing featured the largest diffuse layer specific area capacitance compared with BCC and FCC packings due to larger electric field at the electrode surface for sphere diameter smaller than 40 nm.
6. The diffuse layer specific area capacitance of closely packed dense spheres and mesopores reached the same asymptotic value corresponding to that of planar electrodes when sphere and pore diameter was larger than 40 and 10 nm, respectively.

Acknowledgments

This material is based upon work supported as part of the Molecularly Engineered Energy Materials, an Energy Frontier Research Center funded by the U.S. Department of Energy, Office of Science, Office of Basic Energy Sciences under Award Number DE-SC0001342.

References

- [1] US Department of Energy, Basic Research Needs for Electrical Energy Storage, http://www.er.doe.gov/bes/reports/files/EES_rpt.pdf, 2007.
- [2] P. Simon, Y. Gogotsi, Materials for electrochemical capacitors, *Nature Materials* 7 (11) (2008) 845.
- [3] A.G. Pandolfo, A.F. Hollenkamp, Carbon properties and their role in supercapacitors, *Journal of Power Sources* 157 (1) (2006) 11.
- [4] O. Stern, The theory of the electrolytic double layer, *Zeitschrift für Elektrochemie und angewandte physikalische Chemie* 30 (1924) 508.
- [5] A.J. Bard, L.R. Faulkner, *Electrochemical Methods: Fundamentals and Applications*, John Wiley & Sons, New York, NY, 2001.
- [6] J.H. Masliyah, S. Bhattacharjee, *Electrokinetic and Colloid Transport Phenomena*, John Wiley & Sons, Hoboken, NJ, 2006.
- [7] H.-J. Butt, M. Kappl, *Surface and Interfacial Forces*, Wiley-VCH Verlag GmbH & Co. KGaA, Germany, 2010.
- [8] E. Frackowiak, F. Beguin, Carbon materials for the electrochemical storage of energy in capacitors, *Carbon* 39 (6) (2001) 937.
- [9] E. Frackowiak, Carbon materials for supercapacitor application, *Physical Chemistry Chemical Physics* 9 (15) (2007) 1774.
- [10] Y. Zhang, H. Feng, X. Wu, L. Wang, A. Zhang, T. Xia, H. Dong, X. Li, L. Zhang, Progress of electrochemical capacitor electrode materials: a review, *International Journal of Hydrogen Energy* 34 (11) (2009) 4889.
- [11] L.L. Zhang, X.S. Zhao, Carbon-based materials as supercapacitor electrodes, *Chemical Society Reviews* 38 (9) (2009) 2520.
- [12] H.-J. Liu, W.-J. Cui, L.-H. Jin, C.-X. Wang, Y.-Y. Xia, Preparation of three-dimensional ordered mesoporous carbon sphere arrays by a two-step templating route and their application for supercapacitors, *Journal of Materials Chemistry* 19 (22) (2009) 3661.
- [13] M. Endo, T. Maeda, T. Takeda, Y.J. Kim, K. Koshiba, H. Hara, M.S. Dresselhaus, Capacitance and pore-size distribution in aqueous and nonaqueous electrolytes using various activated carbon electrodes, *Journal of the Electrochemical Society* 148 (8) (2001) 910.
- [14] C. Vix-Guterl, E. Frackowiak, K. Jurewicz, M. Friebe, J. Parmentier, F. Beguin, Electrochemical energy storage in ordered porous carbon materials, *Carbon* 43 (6) (2005) 1293.
- [15] A.B. Fuertes, G. Lota, T.A. Centeno, E. Frackowiak, Templated mesoporous carbons for supercapacitor application, *Electrochimica Acta* 50 (14) (2005) 2799.
- [16] W. Xing, S.Z. Qiao, R.G. Ding, F. Lid, G.Q. Lu, Z.F. Yan, H.M. Cheng, Superior electric double layer capacitors using ordered mesoporous carbons, *Carbon* 44 (2) (2006) 216.
- [17] E. Raymundo-Pinero, K. Kierzek, J. Machnikowski, F. Beguin, Relationship between the nanoporous texture of activated carbons and their capacitance properties in different electrolytes, *Carbon* 44 (12) (2006) 2498.
- [18] J. Chmiola, G. Yushin, Y. Gogotsi, C. Portet, P. Simon, P.L. Taberna, Anomalous increase in carbon capacitance at pore sizes less than 1 nanometer, *Science* 313 (5794) (2006) 1760.
- [19] M. Sevilla, S. Alvarez, T.A. Centeno, A.B. Fuertes, F. Stoeckli, Performance of templated mesoporous carbons in supercapacitors, *Electrochimica Acta* 52 (9) (2007) 3207.
- [20] C. Portet, G. Yushin, Y. Gogotsi, Effect of carbon particle size on electrochemical performance of EDLC, *Journal of the Electrochemical Society* 155 (7) (2008) 531.
- [21] C. Largeot, C. Portet, J. Chmiola, P.-L. Taberna, Y. Gogotsi, P. Simon, Relation between the ion size and pore size for an electric double-layer capacitor, *Journal of the American Chemical Society* 130 (9) (2008) 2730.
- [22] J. Chmiola, C. Largeot, P.-L. Taberna, P. Simon, Y. Gogotsi, Desolvation of ions in subnanometer pores and its effect on capacitance and double-layer theory, *Angewandte Chemie International Edition* 47 (18) (2008) 3392.
- [23] R. Lin, P.L. Taberna, J. Chmiola, D. Guay, Y. Gogotsi, P. Simon, Microelectrode study of pore size, ion size, and solvent effects on the charge/discharge behavior of microporous carbons for electrical double-layer capacitors, *Journal of the Electrochemical Society* 156 (1) (2009) 7.
- [24] J.A. Fernandez, S. Tennison, O. Kozynchenko, F. Rubiera, F. Stoeckli, T.A. Centeno, Effect of mesoporosity on specific capacitance of carbons, *Carbon* 47 (6) (2009) 1598.
- [25] D. Banham, F. Feng, J. Burt, E. Alsayheem, V. Birss, Bimodal, templated mesoporous carbons for capacitor applications, *Carbon* 48 (4) (2010) 1056.
- [26] F. Li, N. van der Laak, S.-W. Ting, K.-Y. Chan, Varying carbon structures templated by KIT-6 for optimum electrochemical capacitance, *Electrochimica Acta* 55 (8) (2010) 2817.
- [27] J. Huang, B.G. Sumpter, V. Meunier, Theoretical model for nanoporous carbon supercapacitors, *Angewandte Chemie International Edition* 47 (3) (2008) 520.
- [28] J. Huang, B.G. Sumpter, V. Meunier, A universal model for nanoporous carbon supercapacitors applicable to diverse pore regimes, carbon materials, and electrolytes, *Chemistry—A European Journal* 14 (22) (2008) 6614.
- [29] B.E. Conway, W.G. Pell, Power limitations of supercapacitor operation associated with resistance and capacitance distribution in porous electrode devices, *Journal of Power Sources* 105 (2) (2002) 169.
- [30] S. Yoon, J.H. Jang, B.H. Ka, S.M. Oh, Complex capacitance analysis on rate capability of electric-double layer capacitor (EDLC) electrodes of different thickness, *Electrochimica Acta* 50 (11) (2005) 2255.

- [31] S. Yoon, C.W. Lee, S.M. Oh, Characterization of equivalent series resistance of electric double-layer capacitor electrodes using transient analysis, *Journal of Power Sources* 195 (13) (2010) 4391.
- [32] M. Kaus, J. Kowa, D.U. Sauer, Modelling the effects of charge redistribution during self-discharge of supercapacitors, *Electrochimica Acta* 55 (25) (2010) 7516.
- [33] J.S. Newman, K.E. Thomas-Alyea, *Electrochemical Systems*, 3rd edition, John Wiley & Sons, Hoboken, NJ, 2004.
- [34] A.M. Johnson, J. Newman, Desalting by means of porous carbon electrodes, *Journal of the Electrochemical Society* 118 (3) (1971) 510.
- [35] B. Pillay, J. Newman, The influence of side reactions on the performance of electrochemical double-layer capacitors, *Journal of the Electrochemical Society* 143 (6) (1996) 1806.
- [36] B. Pillay, Design of electrochemical capacitors for energy storage, Ph.D. Thesis, Department of Chemical Engineering, University of California, Berkeley, CA, 1996.
- [37] I.J. Ong, J. Newman, Double-layer capacitance in a dual lithium ion insertion cell, *Journal of the Electrochemical Society* 146 (12) (1999) 4360.
- [38] V. Srinivasan, J.W. Weidner, Mathematical modeling of electrochemical capacitors, *Journal of the Electrochemical Society* 146 (5) (1999) 1650.
- [39] C. Lin, J.A. Ritter, B.N. Popov, R.E. White, A mathematical model of an electrochemical capacitor with double-layer and Faradaic processes, *Journal of the Electrochemical Society* 146 (9) (1999) 3168.
- [40] C. Lin, B.N. Popov, H.J. Ploehn, Modeling the effects of electrode composition and pore structure on the performance of electrochemical capacitors, *Journal of the Electrochemical Society* 149 (2) (2002) 167.
- [41] D. Dunn, J. Newman, Predictions of specific energies and specific powers of double-layer capacitors using a simplified model, *Journal of the Electrochemical Society* 147 (3) (2000) 820.
- [42] H. Kim, B.N. Popov, A mathematical model of oxide, carbon composite electrode for supercapacitors, *Journal of the Electrochemical Society* 150 (9) (2003) 1153.
- [43] G. Sikha, R.E. White, B.N. Popov, A mathematical model for a lithium-ion battery/electrochemical capacitor hybrid system, *Journal of the Electrochemical Society* 152 (8) (2005) 1682.
- [44] M.W. Verbrugge, P. Liu, Microstructural analysis and mathematical modeling of electric double-layer supercapacitors, *Journal of the Electrochemical Society* 152 (5) (2005) 79.
- [45] S.A. Kazaryan, S.N. Razumov, S.V. Litvinenko, G.G. Kharisov, V.I. Kogan, Mathematical model of heterogeneous electrochemical capacitors and calculation of their parameters, *Journal of the Electrochemical Society* 153 (9) (2006) 1655.
- [46] S.K. Griffiths, R.H. Nilson, Optimum interparticle porosity for charge storage in a packed bed of nanoporous particles, *Journal of the Electrochemical Society* 157 (4) (2010) 469.
- [47] M.Z. Bazant, K. Thornton, A. Ajdari, Diffuse-charge dynamics in electrochemical systems, *Physical Review E* 70 (2) (2004) 1 (No. 021506).
- [48] K.T. Chu, M.Z. Bazant, Nonlinear electrochemical relaxation around conductors, *Physical Review E* 74 (1) (2006) 1 (No. 011501).
- [49] L.H. Olesen, M.Z. Bazant, H. Bruus, Strongly nonlinear dynamics of electrolytes in large ac voltages, *Physical Review E* 82 (1) (2006) 1 (No. 011501).
- [50] L. Yang, B.H. Fishbine, A. Migliori, L.R. Pratt, Molecular simulation of electric double-layer capacitors based on carbon nanotube forests, *Journal of the American Chemical Society* 131 (34) (2009) 12373.
- [51] K. Tonurist, A. Janes, T. Thomberg, H. Kurig, E. Lust, Influence of mesoporous separator properties on the parameters of electrical double-layer capacitor single cells, *Journal of the Electrochemical Society* 156 (4) (2009) 334.
- [52] J.J. Bikerman, Structure and capacity of electrical double layer, *Philosophical Magazine* 33 (220) (1942) 384.
- [53] I. Borukhov, D. Andelman, H. Orland, Steric effects in electrolytes: a modified Poisson–Boltzmann equation, *Physical Review Letters* 79 (3) (1997) 435.
- [54] M.S. Kilic, M.Z. Bazant, A. Ajdari, Steric effects in the dynamics of electrolytes at large applied voltages. I. Double-layer charging, *Physical Review E* 75 (2) (2007) 1 (No. 021502).
- [55] M.Z. Bazant, M.S. Kilic, B.D. Storey, A. Ajdari, Towards an understanding of induced-charge electrokinetics at large applied voltages in concentrated solutions, *Advances in Colloid and Interface Science* 152 (1–2) (2009) 48.
- [56] B.E. Conway, *Electrochemical Supercapacitors: Scientific Fundamentals and Technological Applications*, Kluwer Academic/Plenum Publishers, New York, NY, 1999.
- [57] R. Qiao, N.R. Aluru, Ion concentrations and velocity profiles in nanochannel electroosmotic flows, *Journal of Chemical Physics* 118 (10) (2003) 4692.
- [58] H. Daiguji, Ion transport in nanofluidic channels, *Chemical Society Reviews* 39 (3) (2010) 901.
- [59] J.C.T. Eijkel, A. van den Berg, Nanofluidics and the chemical potential applied to solvent and solute transport, *Chemical Society Reviews* 39 (3) (2010) 957.
- [60] W. Sparreboom, A. van den Berg, J.C.T. Eijkel, Transport in nanofluidic systems: a review of theory and applications, *New Journal of Physics* 12 (1) (2010) 1 (No. 015004).
- [61] P.M. Biesheuvel, M. van Soestbergen, Counterion volume effects in mixed electrical double layers, *Journal of Colloid and Interface Science* 316 (2) (2007) 490.
- [62] A.A. Kornyshev, Double-layer in ionic liquids: paradigm change? *Journal of Physical Chemistry B* 111 (20) (2007) 5545.
- [63] A.D. Buckingham, Theory of the dielectric constant at high field strengths, *Journal of Chemical Physics* 25 (3) (1956) 1 (No. 428).
- [64] I.-C. Yeh, M.L. Berkowitz, Dielectric constant of water at high electric fields: molecular dynamics study, *Journal of Chemical Physics* 110 (16) (1999) 1 (No. 7935).
- [65] A.J. Appleby, Electron transfer reactions with and without ion transfer, in: B.E. Conway, C.G. Vayenas, R.E. White, M.E. Gamboa-Adelco (Eds.), *Modern Aspects of Electrochemistry*, No. 38, Kluwer Academic/Plenum Publishers, New York, NY, 2005, p. 175.
- [66] F. Booth, The dielectric constant of water and the saturation effect, *Journal of Chemical Physics* 19 (4) (1951) 391.
- [67] F. Booth, Dielectric constant of polar liquids at high field strengths, *Journal of Chemical Physics* 23 (3) (1955) 453.
- [68] Y. Gur, I. Ravina, A.J. Babchin, On the electrical double layer theory. II. The Poisson–Boltzmann equation including hydration forces, *Journal of Colloid and Interface Science* 64 (2) (1978) 333.
- [69] S. Basu, M.M. Sharma, Effect of dielectric saturation on disjoining pressure in thin films of aqueous electrolytes, *Journal of Colloid and Interface Science* 165 (2) (1994) 355.
- [70] V.N. Paunov, R.I. Dimova, P.A. Kralchevsky, G. Broze, A. Mehreteab, The hydration repulsion between charged surfaces as an interplay of volume exclusion and dielectric saturation effects, *Journal of Colloid and Interface Science* 182 (1) (1996) 239.
- [71] G.J. Janz, R.P.T. Tomkins, *Nonaqueous Electrolytes Handbook*, vol. I, Academic Press, New York, NY, 1972.
- [72] G. Mousouzias, G. Ritzoulis, Relative permittivities and refractive indices of propylene carbonate + toluene mixtures from 283.15 K to 313.15 K, *Journal of Chemical & Engineering Data* 42 (4) (1997) 710.
- [73] L. Yang, B.H. Fishbine, A. Migliori, L.R. Pratt, Dielectric saturation of liquid propylene carbonate in electrical energy storage applications, *Journal of Chemical Physics* 132 (4) (2010) 1 (No. 044701).
- [74] M. Ue, K. Ida, S. Mori, Mobility and ionic association of lithium and quaternary ammonium salts in propylene carbonate and γ -butyrolactone, *Journal of the Electrochemical Society* 141 (12) (1994) 3336.
- [75] J.N. Israelachvili, *Intermolecular and Surface Forces*, 2nd edition, Academic Press, San Diego, CA, 1992.
- [76] B.E. Conway, *Electrolyte solutions: solvation and structural aspects*, *Annual Review of Physical Chemistry* 17 (1966) 481.
- [77] Y. Marcus, Ionic radii in aqueous solutions, *Chemical Reviews* 88 (8) (1988) 1475.
- [78] V.N. Afanasev, A.N. Ustinov, Adiabatic compressibility of hydrated complexes of electrolytes, *Electrochimica Acta* 54 (26) (2009) 6455.
- [79] M. Noked, E. Avraham, A. Soffer, D. Aurbach, Assessing the concentration effect on hydration radii in aqueous solutions by electroadsorption on a carbon molecular sieve electrode, *Journal of Physical Chemistry C* 114 (31) (2010) 13354.
- [80] N. Nanbu, T. Ebina, H. Uno, S. Ishizawa, Y. Sasaki, Physical and electrochemical properties of quaternary ammonium bis(oxalato)borates and their application to electric double-layer capacitors, *Electrochimica Acta* 52 (4) (2006) 1763.
- [81] D.J. Griffiths, *Introduction to Electrodynamics*, 3rd edition, Prentice Hall, Upper Saddle River, NJ, 1999.